Hindawi
Advances in Materials Science and Engineering
Volume 2022, Article ID 6244566, 10 pages
https://doi.org/10.1155/2022/6244566

*Research Article*

# Fracture Behavior of Ion-Nitrided AISI 4140 Steel in accordance with Variable Applied Current Density

**Hyun Jun Park,[1,2] Bum Soo Kim,[1] Chi Sung Ahn,[1] Kyun Taek Cho,[3] Kyoung Il Moon ,[1] and Sang Sub Kim [2]**

[1]*Heat & Surface Technology R&D Department, Korea Institute of Industrial Technology, 113-58, Seohaean-ro, Gyeonggi-do, Siheung-si 15014, Republic of Korea*
[2]*Department of Materials Science and Engineering, Inha University, Incheon 402-751, Republic of Korea*
[3]*Automotive Materials & Components R&D Department, Korea Institute of Industrial Technology, 34 Haeryongsandan 2-ro Haeryong-myeon, Jeollanam-do, Suncheon-si 58022, Republic of Korea*

Correspondence should be addressed to Kyoung Il Moon; kimoon@kitech.re.kr and Sang Sub Kim; sangsub@inha.ac.kr

Received 4 March 2022; Revised 18 May 2022; Accepted 30 May 2022; Published 15 July 2022

Academic Editor: Hongchao Kou



In this study, the fracture behavior of AISI 4140 low-alloy steel nitrided with respect to the applied current density was investigated. A series of rotary bending fatigue tests were performed with various loads (350, 400, 450, and 500 N) at a constant rotational speed of 2000 rpm. The results show that the increase in the fatigue strength of the steel (up to 35%) strongly depends on the compound layer formed during the nitriding process. In addition, the compressive stress generated by nitrogen-ion bombardment and implantation had an advantageous effect on the substantially enhanced fatigue strength; it acted as a protective layer to secure the surface from any external impact. It was found that fatigue strength is increased with increasing fracture toughness index on the surface on the sample. It had the highest fracture toughness index and fatigue strength at about 0.85 mA/cm$^2$ of applied current. The findings of this study will pave the way for applications in related industries.

## 1. Introduction

Ion nitriding is a popular glow-discharge surface modification treatment employed to enhance the fatigue strength, wear properties, and surface hardness of ferrous alloys [1, 2]. A nitrogen diffusion layer of approximately 200–400 $\mu$m is formed during the nitriding process for parts made of AISI 4140 low-alloy steel, such as bearings and gears [2]. In this process, nitrogen diffuses into the surface region of the material and a compound layer is formed by combining nitrogen ($\varepsilon$-$Fe_{2\text{-}3}N$ and $\gamma'$-$Fe_4N$) with the alloying elements of the matrix on the surface of the material. Nitriding has been widely employed, particularly because it is advantageous to obtain hard surface layers without any modification to the bulk material properties [3].

In the ion nitriding process, compound and nitrogen diffusion layer are formed with high compressive residual stress on the surface of steel. The compressive residual stress induced in the nitrided layer enhances the surface hardness, wear, corrosion resistance, and fatigue strength. Fatigue behavior generally originates from the surface and/or near surface on the material [4–6]. The crack starts at the interface between the high and low residual stress sites owing to the compressed residual stress in the diffusion layer [1, 5]. Several researchers have studied the fatigue behavior of various steels subjected to ion nitriding. They reported that the fatigue life period increases with increasing case depth and surface hardness; however, the thickness of the compound layer does not affect the fatigue limit [2, 7, 8]. A diffusion layer formed during the ion nitriding process causes compressive residual stress on the surface of the specimens. It improves the fatigue life; a hard layer is formed owing to the increased residual stress, which prevents plastic deformation. However, previous

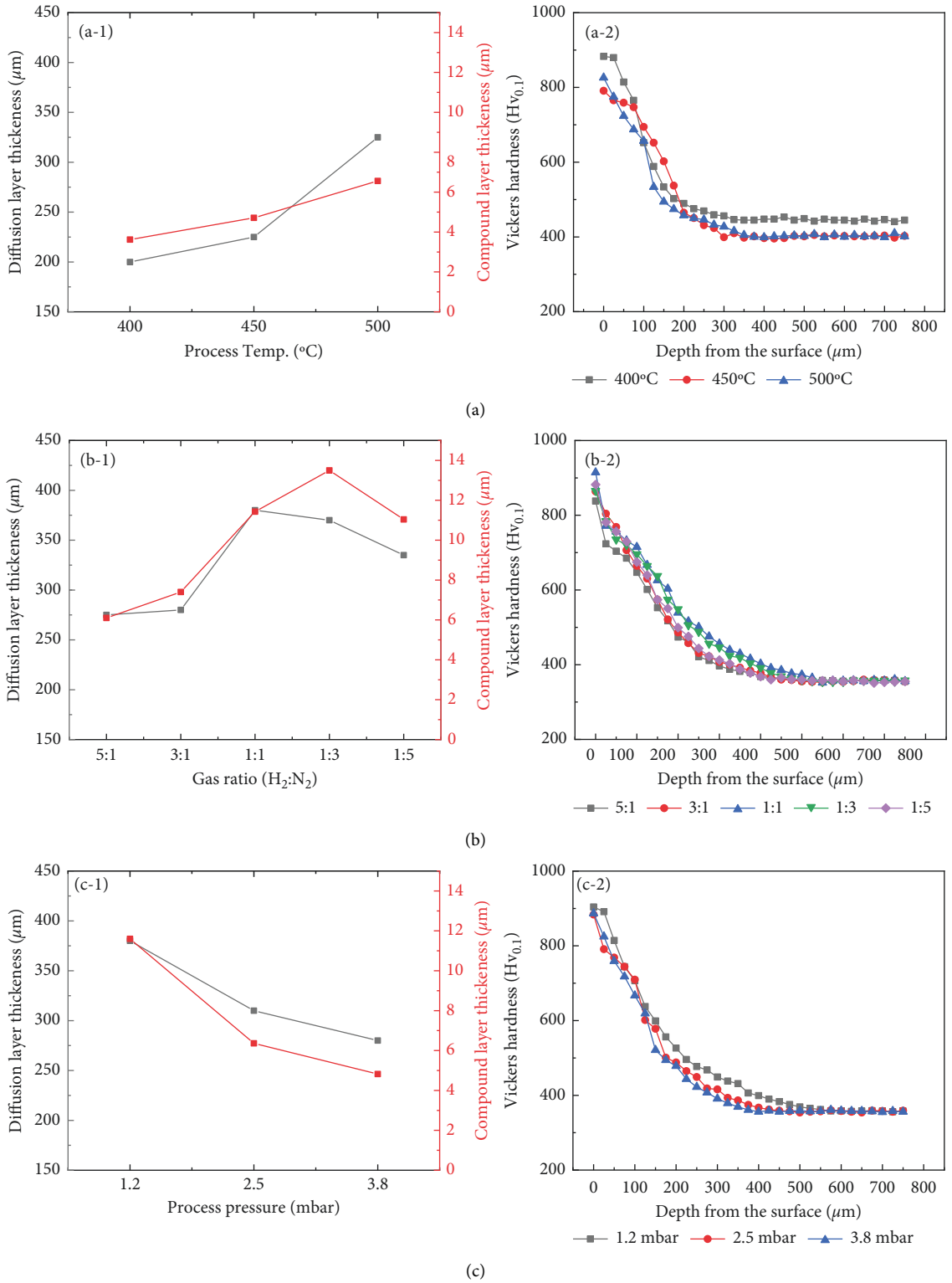


FIGURE 1: Thickness of compound layer and nitrogen diffusion layer. The first column (a-1, b-1, c-1) represents formed layer thickness, while the second column (a-2, b-2, c-2) represents hardness profiles. From top to bottom, the sequence of the rows is process temperature, process gas ratio, and process pressure.

studies [2, 7–11] have not investigated the effect of the thickness of the compound layer with a similar diffusion layer. It has only been reported that the fatigue strength increases with the thickness of the nitrogen diffusion layer because the fatigue crack initiation site moves further into the core.

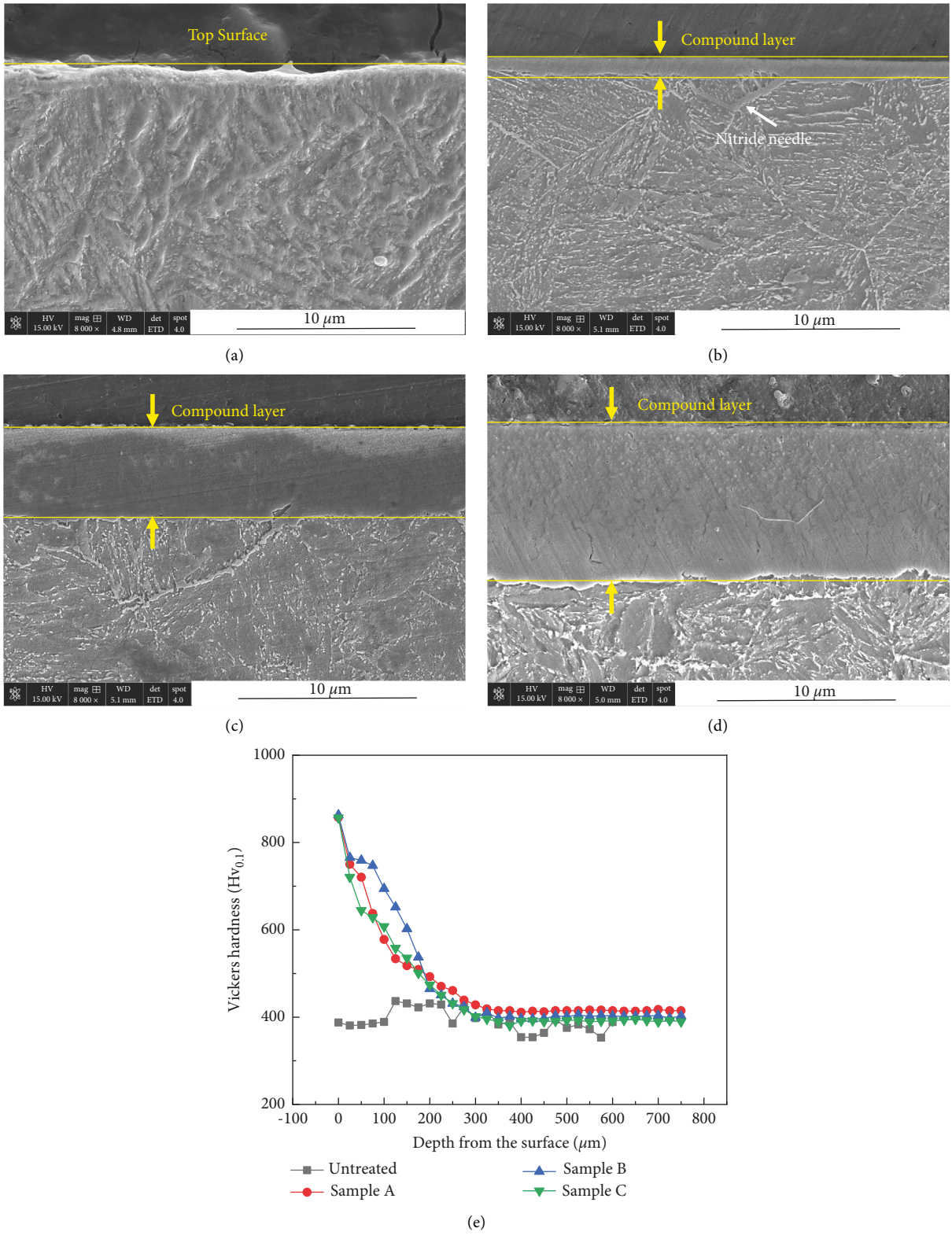


Figure 2: SEM images and hardness profiles of the cross-sectional microstructure of (a) Untreated, (b) Sample A, (c) Sample B, and (d) Sample C. (e) Vickers hardness profiles.

In this study, we report the fatigue characteristics of AISI 4140 specimens nitrided at different current densities. The case depth is parabolically related to the nitriding time and temperature [12–14]; therefore, a long treatment time is required to deepen the case depth to increase fatigue strength. Should the fatigue strength be affected by the

compound layer, however, it is expected to reduce production costs resulting from decreased nitriding process time. This contribution contains results of effect of compound layer of nitrided samples on fatigue resistance of AISI 4140 low-alloy steel.

## 2. Results and Discussion

In DC (direct current) pulsed plasma nitriding, the trends of nitride layer formation with various factors are shown in Figure 1. In previous studies, the thickness of the compound layer and the nitrogen diffusion layer increased linearly as the process temperature (Figure 1(a)) increased. According to the process gas ratio of $H_2/N_2$ (Figure 1(b)), the thickness of the compound layer and nitrogen diffusion layer increased with increasing nitrogen content up to 1 : 3, whereas it decreased when a nitrogen atmosphere over 85% was used. In addition, the lower the process pressure (Figure 1(c)) [14], the greater the thickness of the compound layer, the thickness of the compound layer was thicker. However, it was confirmed that the applied current density was the largest variable in the thickness of the composite layer when compared with the process temperature, gas ratios, and pressures during the same process time [15].

Figure 2 shows the scanning electron microscopy (SEM) images and the hardness profiles of the cross-sectional microstructure of the untreated and ion-nitrided specimens in response to different applied current densities. The hardness profile of cross section of the untreated sample was shown as trend of general Q/T AISI 4140 steel with hardness of about 400 HV0.1. On the other hand, the structure of the compound layer attained during the ion nitriding of AISI 4140 was highly dependent on the applied current density. The thickness of the compound layer increases to 1 $\mu$m, 5 $\mu$m, and 10 $\mu$m as the current density increases to 0.43 mA/cm$^2$, 0.85 mA/cm$^2$, and 1.27 mA/cm$^2$, respectively, as shown in Figures 2(a)–2(d). The current density increased, and the nitride needles in the grain boundaries tended to become thicker. The hardness profiles of the nitrided samples are shown in Figure 2(e). Beneath the surface, the hardness of the nitrided samples was found to be approximately 860 HV0.1, whereas the core was characterized by significantly lower values of approximately 400 HV0.1. The hardness decreased as the hardness measurement point moved toward the core, and it can be estimated from the hardness profile that the thickness of the hardened layer was approximately 210 $\mu$m.

The crystallographic characteristics of the untreated and nitrided specimens are shown in Figure 3. The compound layer consisted predominantly of ɣ-$Fe_4N$ with traces of ε-$Fe_{2\text{-}3}N$ in all nitrided samples. As can be observed, the ε-$Fe_{2\text{-}3}N$ phase was detected at angles of approximately 37°, 43°, 58°, and 78° in Sample A. In contrast, the ɣ-$Fe_4N$ phase was confirmed at angles of around 41°, 48°, 70°, and 84° in Samples B and C. Additionally, the ε-$Fe_{2\text{-}3}N$ phases of Samples B and C were weakly confirmed only at an angle of 37° [16, 17]. Sample A test piece had the highest ε-$Fe_{2\text{-}3}N$ peak. Samples B and C had the highest ɣ-$Fe_4N$ peak because nitrogen diffusion into the base metal is a reactive diffusion,

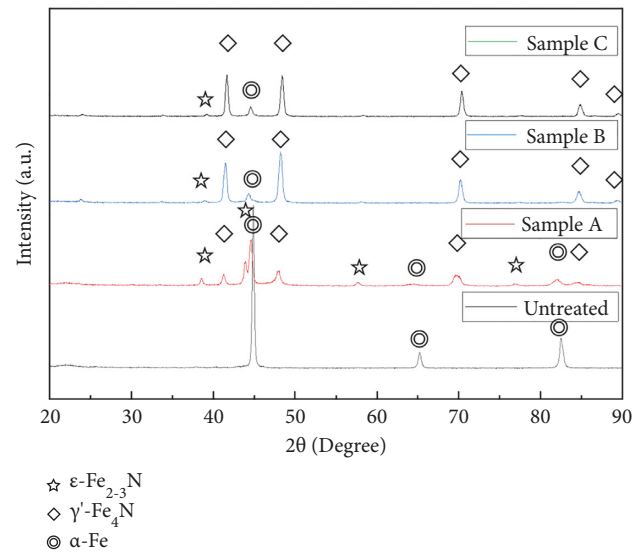


Figure 3: XRD patterns of the untreated and ion-nitrided specimens.

as with increasing nitrogen concentration in the substrate, there is a change in phase composition [18].

The fracture surface and fatigue strength of AISI 4140 steel are shown in Figures 4(a)–4(d) and Figure 4(e), respectively. In the base metal (Figure 4(a)) and Sample A (Figure 4(b)), a portion of the outermost surface was torn off at the part where the ductile fracture had developed [19]. Notably, the fish eye was not formed in the base metal, whereas it was formed in all the nitrided specimens. All the nitride specimens exhibited internal cracking [9]. The points of formation of the fish eye were approximately 440 $\mu$m, 466 $\mu$m, and 458 $\mu$m away from the surface for Samples A, B, and C, respectively. Metal oxide inclusions, such as compounds of Fe, Cr, and Zn, were generated in the center of the fish eye [20]. Samples A, B, and C (Figures 4(b)–4(d), respectively) exhibited a brittle fracture pattern in which a typical fish eye was formed and the sizes of the inclusions were approximately 12 $\mu$m, 78 $\mu$m, and 26 $\mu$m, respectively. The untreated sample did not fracture at loads up to 634 MPa. Samples A, B, and C did not fracture until 683 MPa, 878 MPa, and 732 MPa, respectively. The untreated sample was fractured at 291,200 cycles under a load of 682 MPa, and fractures of Samples A and C occurred at 5,523,200 cycles and 1,217,500, respectively, each under a load of 780 MPa. In particular, Sample B failed abruptly at 367,700 cycles under a load of 926 MPa because surface crack propagates through the core under high loads [21].

Figure 5 shows an optical microscope image representing the indentation produced by subjecting the base metal and the surface of the nitride-treated specimen to a load of 490 N. The challenges in accurately determining the Vickers indentation fracture toughness include accounting for the type of cracks formed, ensuring a precise measurement of the crack length, and selecting a suitable equation. In Figure 5(b), "a" is half the diagonal length of the indentation edge, "ℓ" is the length of the crack generated in

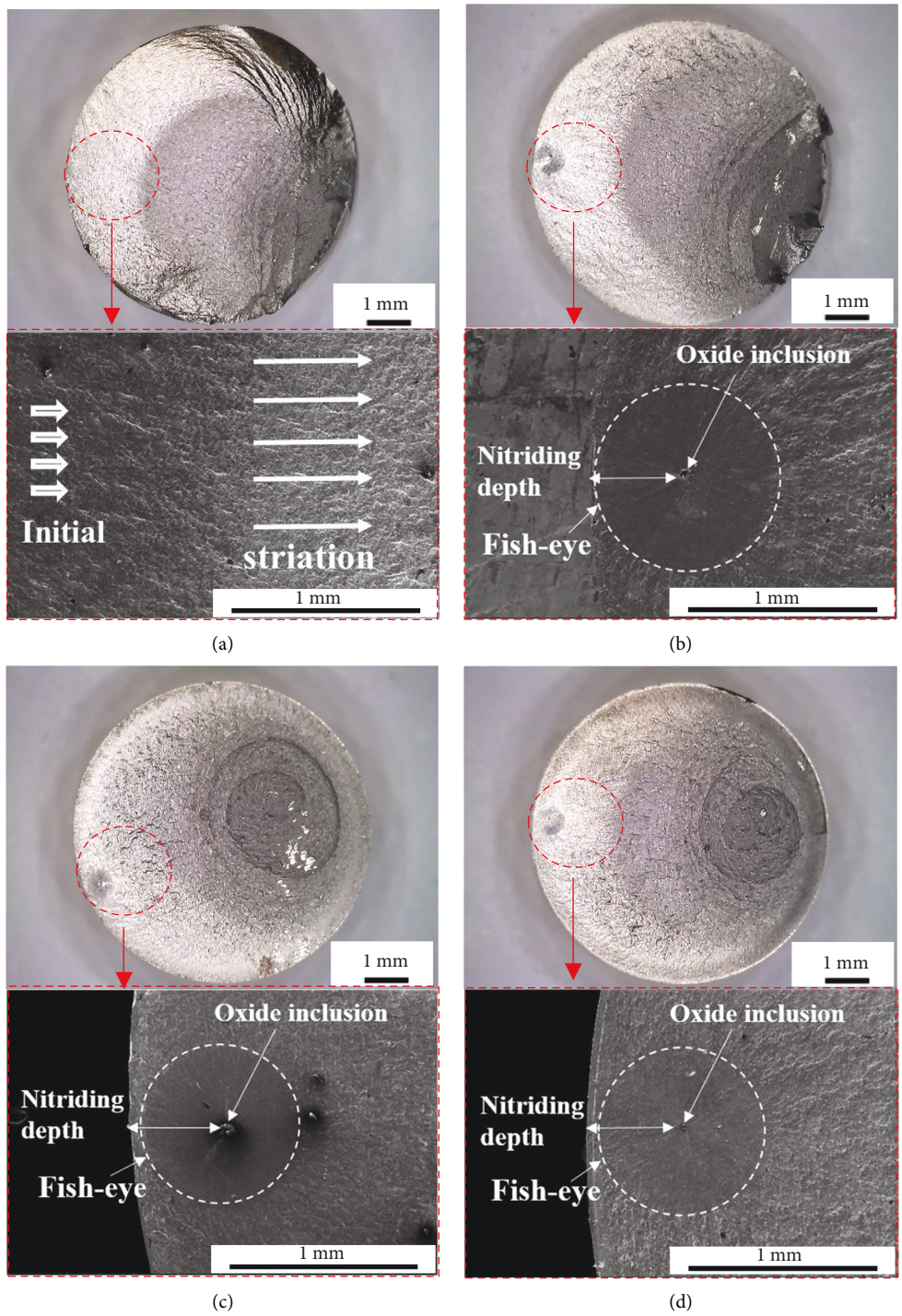


the indentation edge, and "c" is the crack length from the center of the indentation to the crack tip ($a + \ell$). If the c/a ratio is less than 2.5, the material shows Palmqvist cracks [22–25]. Table 1 presents the results of the fracture toughness index ($K_{Ic}$) according to the applied load. For all the nitrided samples, Palmqvist cracks were observed under all indentation loads, that is, the c/a ratio was less than 2.5 (Table 1). The fracture toughness index can be calculated by the following equation:

$$K_{Ic} = 0.0319 \cdot \left(F/\left(a \cdot \ell^{1/2}\right)\right), \quad (1)$$

where F is the load applied during the Vickers test (N). In the base metal (Figure 5(a)), owing to the ductility of the material, "a" was approximately 230 $\mu$m, and the indentation periphery was depressed without the occurrence of cracks. As shown in Figure 5(b), "a" of the Sample A was approximately 230 $\mu$m, and cracks with lengths of 26–66 $\mu$m were formed. Figures 5(c) and 5(d) show that "a" of Samples

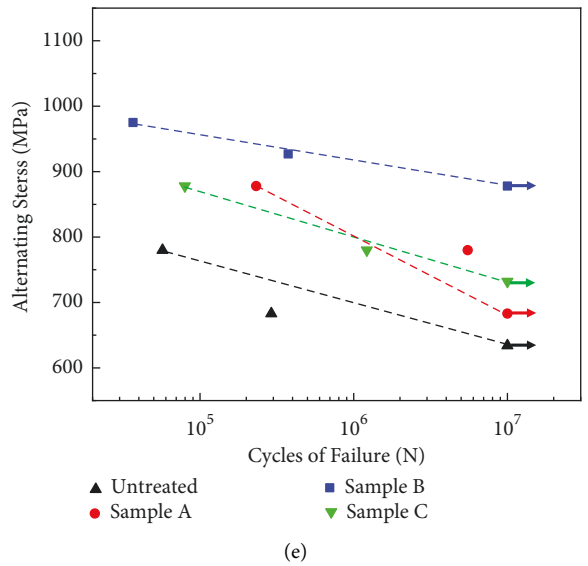


(e)

Figure 4: SEM fractographs. (a) Untreated sample, 682 MPa, 291,200 cycles, air. (b) Sample A, 780 MPa, 5,523,200 cycles, air. (c) Sample B, 926 MPa, 367,700 cycles, air. (d) Sample C, 780 MPa, 1,217,500 cycles, air. (e) S-N curves of fatigue test.

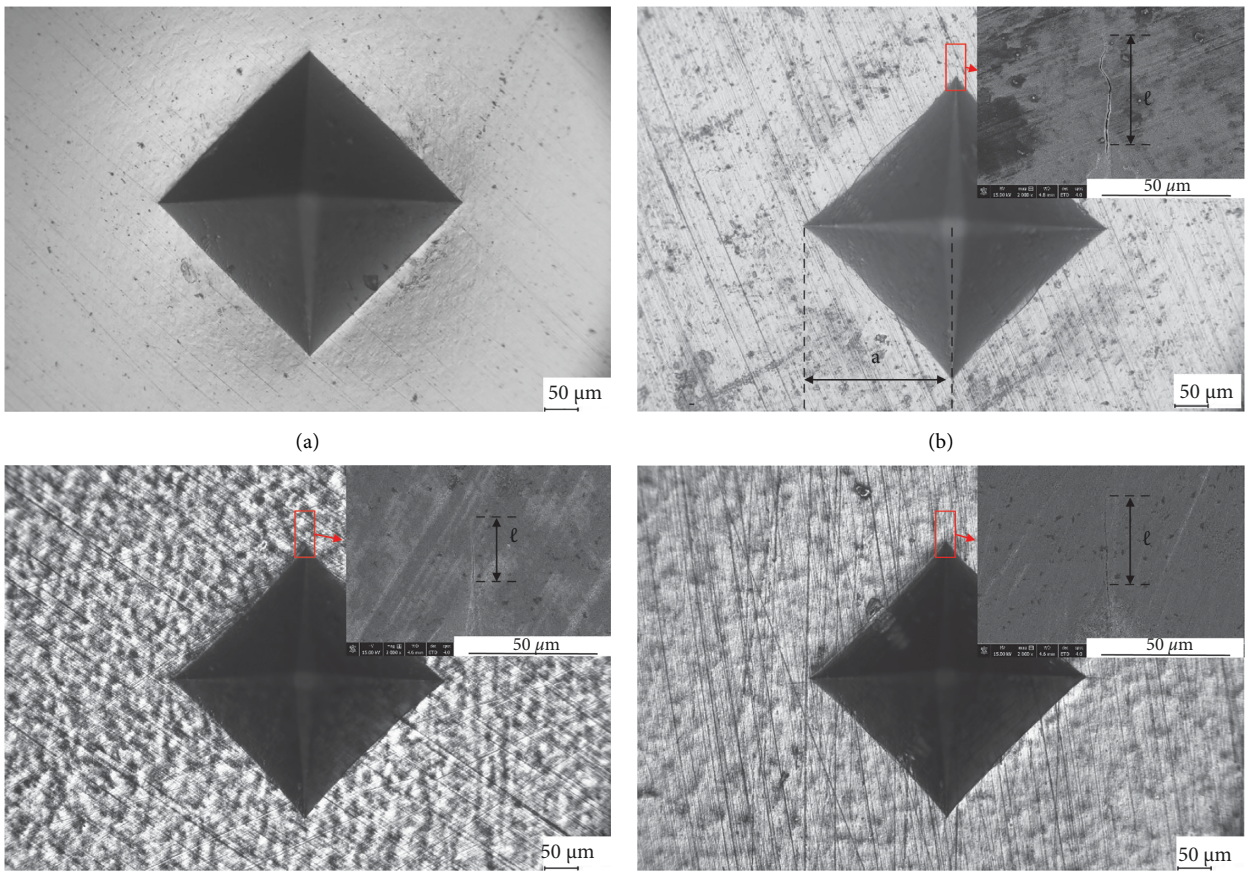


Figure 5: Micrographs of the Vickers indentation and cracks at test loads of 490 N. (a) Untreated. (b) Sample A. (c) Sample B. (d) Sample C.

B and C was approximately 210 $\mu$m; however, Sample B had an average crack length "ℓ" of 20 $\mu$m, while Sample C had the greatest "ℓ" of 36 $\mu$m.

To investigate the fracture toughness of the nitride specimens, a macro Vickers hardness tester was used to apply loads of 29.42, 98, 294, and 490 N, as shown in

Table 1: Statistical analysis of the indentation fracture toughness ($K_{Ic}$) of nitrided AISI 4140 steel as a function of the test load, using the equation of Shetty et al.

| Specimen | F, N | c/a | $K_{Ic}$, MPa $m^{1/2}$ | | |
|---|---|---|---|---|---|
| | | | Average | Min. | Max. |
| Sample A | 29.42 | 1.06–1.20 | 8.89 | 6.86 | 11.87 |
| | 98 | 1.09–1.16 | 10.47 | 9.03 | 11.79 |
| | 294 | 1.13–1.22 | 10.62 | 8.77 | 11.55 |
| | 490 | 1.12–1.29 | 11.30 | 8.25 | 13.04 |
| Sample B | 29.42 | - | - | - | - |
| | 98 | - | - | - | - |
| | 294 | 1.12–1.14 | 13.12 | 11.72 | 13.69 |
| | 490 | 1.09–1.10 | 16.50 | 15.86 | 16.84 |
| Sample C | 29.42 | - | - | - | - |
| | 98 | - | - | - | - |
| | 294 | 1.18–1.23 | 10.49 | 9.75 | 11.41 |
| | 490 | 1.17–1.18 | 12.33 | 12.17 | 12.46 |

Figure 6. The fracture toughness index was calculated by substituting the length of the cracks and edges of the indentation formed on the surface into the equation proposed by Shetty et al. [26]. For Sample A, cracks started to develop around the indentation owing to a load of 29 N, whereas Sample B and C specimens with a compound layer thickness of 5 $\mu$m or more started cracking at a load of 294 N. The fracture toughness index of Sample A was approximately $10.32 \pm 1$ under all applied loads. Sample C showed fracture toughness indexes of approximately $10.49 \pm 1$ and $12.33 \pm 0.15$ at the applied loads of 294 N and 490 N, respectively. Sample B showed the highest fracture toughness indexes of approximately $13.12 \pm 1.4$ and $16.50 \pm 0.7$ at applied loads of 294 N and 490 N, respectively.

Figure 7 shows the results of the residual stress measurements using X-rays for all specimens. The untreated specimen was subjected to tensile stress at all depths due to formation of oxidation and/or decarburizing during the tempering process, and in particular, a tensile stress of approximately 630 MPa on the surface; thus, fractures easily occurred owing to fatigue. In contrast, all nitrided specimens were subjected to compressive stress due to nitrides between grain and grain boundary. The compressive stress on Sample A was 679 MPa, and as the compound layer thickened, the surface compressive stress increased to 1081 MPa and 1253 MPa for Samples B and C, respectively. Compressive stress was generated up to the depth of nitrogen diffusion in all nitrided specimens. When an internal crack occurred, it was confirmed that the crack propagated slowly with an increase in compressive stress [21].

The fatigue strength of the nitrided specimens was improved by 10% compared to that of the base metal. Moreover, the fatigue strength of the specimens with a compound layer of 5 $\mu$m thick was improved by more than 240 MPa compared with that of the base metal. There are two reasons for the improvement in the fatigue strength of the nitrided specimens. First, the maximum fatigue strength of the nitrided specimens was correlated with the increase in compressive stress owing to nitrogen diffusion into the base

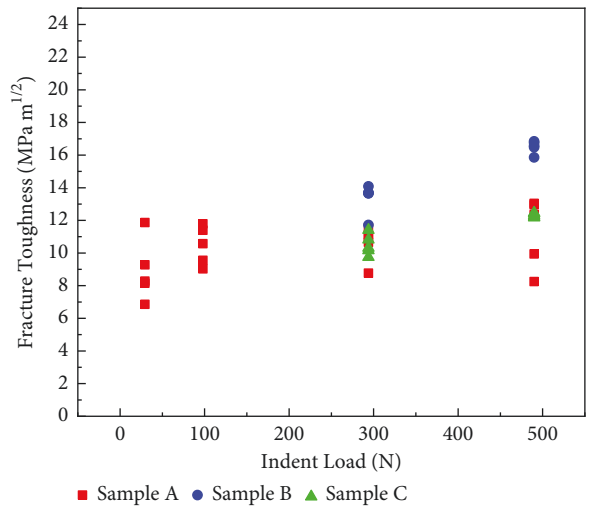


Figure 6: Fracture toughness of the ion-nitrided specimens.

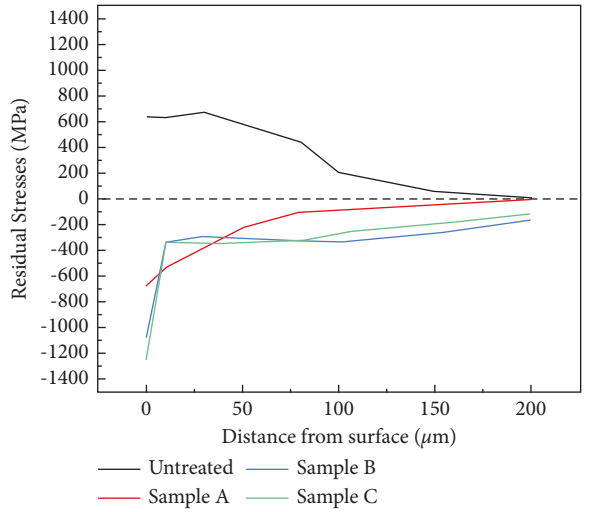


Figure 7: Residual stress depth profiles for the untreated and ion-nitrided specimens.

metal. The hardness and fatigue strength were enhanced owing to the compressive stress generated by nitriding [2, 7, 27–32]. However, it was confirmed that the fatigue strength increased only up to a certain compound layer thickness. That is, the fatigue strength of Sample B was higher than that of Sample C. The fracture toughness index of the compound layer was similar to that of the nitrided specimen. The brittle fracture criteria of the compound layer are not sensitive to the residual stresses when the cracks do not intersect at the grain boundary because the fracture resistance is directly related to the structural nonuniformity of the iron nitride compound layer [33]. That is, $K_{Ic}$ of Sample B was higher than that of Sample C, although the compressive residual stress on the surface of Sample C was the highest. In particular, it was confirmed that the fracture delay occurred in the compound layer and fracture toughness index of Sample B was the highest.

Generally, the fatigue strength of a specimen is reported to increase owing to the nitrogen diffusion layer [34],

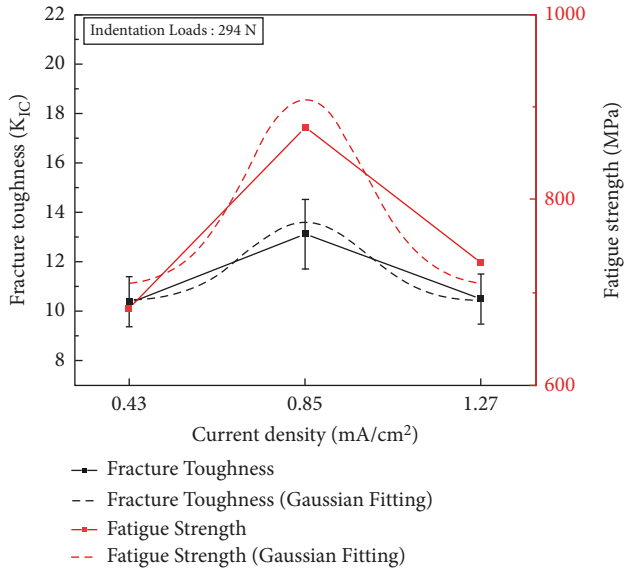


Figure 8: Relation between the fatigue strength and the fracture toughness for the ion-nitrided specimens.

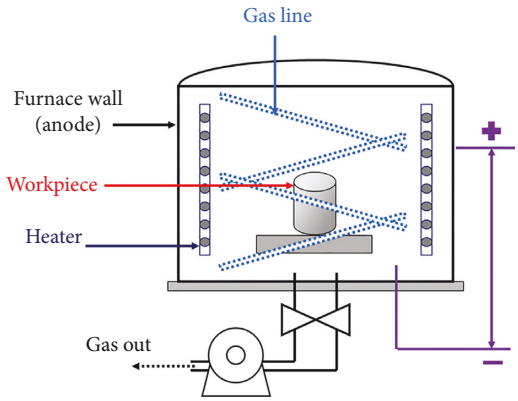


Figure 9: Schematic of the ion-nitriding equipment.

Table 2: Parameters for the ion-nitriding processes.

| Parameter | Condition |
|---|---|
| Base heat treatment | Industrially quenched and tempered (Q/T) |
| Pressure (mbar) | 2.7 |
| Gas ratio ($N_2$ : $H_2$) | 1 : 3 |
| Temperature (°C) | 400 |
| Time (min) | 240 |
| Supplied current density (mA/cm²) | 0.43 (Sample A), 0.85 (Sample B), and 1.27 (Sample C) |

whereas the final fatigue fracture was correlated with the ductility of the compound layer in this study. Thus, it is expected that for a specimen in which a compound layer of a certain thickness is formed, the fracture toughness index of the surface will increase, and the fracture will be delayed. As a summary, Figure 8 shows the relationship between the fatigue strength and fracture toughness as a Gaussian graph. The fatigue strength increased as the fracture toughness index increased owing to the formation of the compound layer.

## 3. Conclusions

We investigated the effect of compound layer thickness on the fatigue strength of ion-nitrided AISI 4140 steel. The effects of the residual stress caused by nitriding and the fracture toughness index of the compound layer were studied. Four types of specimens were prepared for a rotation fatigue test: an untreated sample, in addition to the samples with applied current density of 0.43 mA/cm$^2$ (Sample A), 0.85 mA/cm$^2$ (Sample B), and 1.27 mA/cm$^2$ (Sample C).

The fatigue strength of the nitrided specimens was higher than that of the base metal. In the nitrided specimens, the fish eye formed approximately 400 $\mu$m away from the surface. Sample B exhibited the highest fatigue strength. The fracture toughness results exhibited a similar tendency. In Sample A, cracks started to develop at the indentation edge from an applied load of 29.42 N, and the average fracture toughness index was approximately 10; however, Samples B and C started cracking from an applied load of 294 N and the fracture toughness was approximately 13 and 10, respectively. As the load increased, the fracture toughness index tended to increase as shown in Figure 6 [6].

## 4. Methods

*4.1. Sample Preparation.* Industrially quenched and tempered AISI 4140 steel was used as the base material. The heat treatment process progressed heating at 880°C for 120 min, with oil quenching and tempering at 550°C for 180 min. The core hardness of the base material was approximately 400 HV0.1, and it was fabricated to a disc shape of the size Ø30 × 10 mm. Before the ion nitriding process, all specimens were ground with 220, 800, 1200, and 2000-grade sandpaper.

The specimens for the rotating bending fatigue test were fabricated according to the KS B ISO 1143 : 2003 standards. All the specimens were cleaned in an ultrasonic bath containing ethanol for 10 min.

*4.2. Ion Nitriding Treatments.* The representative ion nitriding equipment is shown in Figure 9. All the specimens were placed on the substrate stage and subjected to cleaning by argon and hydrogen sputtering for 30 min under a voltage of 600 V and pressure of 0.7 mbar to remove surface contaminants. Three levels of ion nitriding were carried out, as listed in Table 2. Ion nitriding was performed under the same process conditions, except for the current density applied to the specimen.

*4.3. Property Measurements*

*4.3.1. Fatigue Strength Test.* After the ion nitriding treatment, the fatigue strength measurements were performed at

a rotational speed of 2000 rpm under atmospheric pressure using rotary bending fatigue testing ($R = -1$) (KDMT-240, Kyung Do Precision Co., Ltd., Republic of Korea). The applied loads were 350 N, 400 N, 450 N, and 500 N at a constant rotational speed of 2000 rpm under ambient conditions of 300 K and approximately $20 \pm 5\%$ humidity. The maximum fatigue strength was determined based on no fracture occurring within 10,000,000 cycles.

*4.3.2. Residual Stress Analysis.* To confirm the residual stresses of all the specimens, the residual stresses of surface and core of the base metal and nitride specimens were measured using a residual stress analyzer (Xstress 3000 G2R, Stresstech) and an X-ray diffractometer (Empyrean, PANalytical).

*4.3.3. Fracture Toughness Calculations.* In the fracture toughness index analysis, a macro Vickers hardness tester was used to apply loads of 29.4, 98, 294, and 490 N to the untreated and nitrided specimens. The fracture toughness index ($K_{Ic}$) was calculated according to the study by Shetty et al., based on the correlation between the Vickers indenter and crack lengths [24].

*4.3.4. Hardness Test.* The nitriding depth and hardness were measured using a Vickers hardness tester (MVK-H1, Mitutoyo) with a test load of 100 g and a dwell time of 10 s. The case depth was defined as a depth of 10% above the core hardness.

*4.3.5. Morphological Measurements of Samples.* To observe the surface compound layer thickness, etching was performed using a nital solution (3% HNO3 + 97% C2H5OH). Thereafter, using a field-emission scanning electron microscope (FEI Nova NanoSEM 450), the measurements were performed at 8000× magnification.

*4.3.6. Surface Phase Analysis of the Samples.* The phase structures on the ion-nitrided surface were determined by XRD (X'pert-Pro MPD, PANalytical). An XRD analysis was performed using a Cu-K$\alpha$ source ($\lambda = 1.541$ Å) and beam intensities of 30 mA and 40 kV.

## Data Availability

No data were used to support this study.

## Conflicts of Interest

The authors declare that they have no conflicts of interest.

## Authors' Contributions

Hyun Jun Park was responsible for conceptualization, investigation, original draft preparation, and review and editing. Bum Soo Kim was responsible for conceptualization and review and editing. Kyun Taek Cho and Chi Sung Ahn were responsible for review and editing. Kyoung Il Moon was responsible for supervision, review and editing, and project administration. Sang Sub Kim was responsible for supervision and review.

## Acknowledgments

This study was supported by the Ministry of Trade, Industry and Energy as a "Technology Innovation Program" (project no. 20011767). This study was also supported by the Korea Institute of Industrial Technology as a "Root Technology Research and Development Project" (kitech EO220005).

## References

[1] H. Kovaci, I. Hacisalihoglu, A. F. Yetim, and A. Celik, "Effect of shot peening pre-treatment and plasma nitriding parameters on the structural, mechanical and tribological properties of AISI 4140 low-alloy steel," *Surface & Coatings Technology*, vol. 358, pp. 256–265, 2019.

[2] A. Alsaran, I. Kaymaz, A. Çelik, F. Yetim, and M. Karakan, "A repair process for fatigue damage using plasma nitriding," *Surface and Coatings Technology*, vol. 186, no. 3, pp. 333–338, 2004.

[3] B. Wang, B. Liu, X. Zhang, and J. Gu, "Enhancing heavy load wear resistance of AISI 4140 steel through the formation of a severely deformed compound-free nitrided surface layer," *Surface and Coatings Technology*, vol. 356, pp. 89–95, 2018.

[4] Z. Xing, Z. Wang, H. Wang, and D. Shan, "Bending fatigue behaviors analysis and fatigue life prediction of 20Cr2Ni4 gear steel with different stress concentrations near non-metallic inclusions," *Materials*, vol. 12, no. 20, p. 3443, 2019.

[5] H. Fu and Y. Liang, "Study of the surface integrity and high cycle fatigue performance of AISI 4340 steel after composite surface modification," *Metals*, vol. 9, no. 8, p. 856, 2019.

[6] F. M. El-Hossary, M. Raaif, A. M. Abd El-Rahman, and M. Abo El-Kassem, "Tribo-mechanical and electrochemical properties of carbonitrided 316 austenitic stainless steel by rf plasma for biomedical applications," *Advances in Materials Physics and Chemistry*, vol. 08, no. 09, pp. 358–377, 2018.

[7] A. Çelik and S. Karadeniz, "Improvement of the fatigue strength of AISI 4140 steel by an ion nitriding process," *Surface and Coatings Technology*, vol. 72, no. 3, pp. 169–173, 1995.

[8] A. Alsaran, M. Karakan, and A. Celik, "Effects of various gas mixtures on plasma nitriding behavior of AISI 5140 steel," *Materials Characterization*, vol. 49, no. 3, pp. 241–246, 2002.

[9] N. Limodin and Y. Verreman, "Fatigue strength improvement of a 4140 steel by gas nitriding: influence of notch severity," *Materials Science and Engineering: A*, vol. 435-436, pp. 460–467, 2006.

[10] I. Cerny and J. Sis, "Fatigue strength of laser harded 42CrMo4 steel considering effects of compressive residual stresses on short crack growth," *Procedia Engineering*, vol. 74, pp. 417–420, 2014.

[11] S. Y. Sirin, K. Sirin, and E. Kaluc, "Effect of the ion nitriding surface hardening process on fatigue behavior of AISI 4340 steel," *Materials Characterization*, vol. 59, no. 4, pp. 351–358, 2008.

[12] P. Cavaliere, A. Perrone, and A. Silvello, "Multi-objective optimization of steel nitriding," *Engineering Science and Technology, an International Journal*, vol. 19, no. 1, pp. 292–312, 2016.

[13] R. R. M. de Sousa, F. O. de Araújo, L. C. Gontijo, J. A. P. da Costa, and C. Alves Jr., "Cathodic cage plasma nitriding (CCPN) of austenitic stainless steel (AISI 316): influence of the different ratios of the (N2/H2) on the nitrided layers properties," *Vacuum*, vol. 86, no. 12, pp. 2048–2053, 2012.

[14] H. F. L. Ramos, A. R. Franco Jr, and E. A. Vieira, "Influence of plasma nitriding pressure on microabrasive wear resistance of a microalloyed steel," *Journal of Materials Research and Technology*, vol. 8, no. 2, pp. 1694–1700, 2019.

[15] S. D. Jacobsen, R. Hinrichs, C. Aguzzoli, C. A. Figueroa, I. J. R. Baumvol, and M. A. Z. Vasconcellos, "Influence of current density on phase formation and tribological behavior of plasma nitrided AISI H13 steel," *Surface and Coatings Technology*, vol. 286, pp. 129–139, 2016.

[16] A. Çelik and S. Karadeniz, "Investigation of compound layer formed during ion nitriding of AISI 4140 steel," *Surface and Coatings Technology*, vol. 80, no. 3, pp. 283–286, 1996.

[17] H. J. Park, H. C. Lee, K. I. Moon, and B. Y. Lee, "Wear properties of a sulfnitrided layer formed on AISI 4140 steel by using plasma treatments," *Journal of the Korean Physical Society*, vol. 74, no. 9, pp. 880–884, 2019.

[18] J. J. Jasinski, T. Fraczek, L. Kurpaska, M. Lubas, and M. Sitarz, "Investigation of nitrogen transport in active screen plasma nitriding processes - uphill diffusion effect," *Journal of Molecular Structure*, vol. 1164, pp. 37–44, 2018.

[19] D. Morin, O. S. Hopperstad, and A. Benallal, "On the description of ductile fracture in metals by the strain localization theory," *International Journal of Fracture*, vol. 209, no. 1-2, pp. 27–51, 2018.

[20] V. F. Terent'ev, M. S. Michugina, A. G. Kolmakov et al., "The effect of nitriding on fatigue strength of structural alloys," *Mechanika*, vol. 2, no. 64, 2007.

[21] N. Limodin, Y. Verreman, and T. Tarfa, "Axial fatigue of a gas-nitrided quenched and tempered AISI 4140 steel: effect of nitriding depth," *Fatigue and Fracture of Engineering Materials and Structures*, vol. 26, no. 9, pp. 811–820, 2003.

[22] K. A. Niihara, "A fracture mechanics analysis of indentation-induced Palmqvist crack in ceramics," *Journal of Materials Science Letters*, vol. 2, no. 5, pp. 221–223, 1983.

[23] Z. Li, A. Ghosh, A. S. Kobayashi, and R. C. Bradt, "Indentation fracture toughness of sintered silicon carbide in the Palmqvist crack regime," *Journal of the American Ceramic Society*, vol. 72, no. 6, pp. 904–911, 1989.

[24] G. D. Quinn, "Fracture toughness of ceramics by the Vickers indentation crack length method: a critical review," *Ceramic Engineering and Science Proceedings*, vol. 27, pp. 45–62, 2007.

[25] M. Bhat, B. Kaur, R. Kumar, K. K. Bamzai, P. N. Kotru, and B. M. Wanklyn, "Effect of ion irradiation on dielectric and mechanical characteristics of ErFeO3 single crystals," *Nuclear Instruments and Methods in Physics Research Section B: Beam Interactions with Materials and Atoms*, vol. 234, no. 4, pp. 494–508, 2005.

[26] A. Sakar-Deliormanli and M. Guden, "Microhardness and fracture toughness of dental materials by indentation method," *Journal of Biomedical Materials Research Part B: Applied Biomaterials*, vol. 76, pp. 257–264, 2006.

[27] N. Yan, R. I. Murakami, and I. S. Lee, "Fatigue behavior of plasma radical nitrided SCM435 steel in super-long life regime," *Metals and Materials International*, vol. 17, no. 4, pp. 577–581, 2011.

[28] S. G. S. Raman and M. Jayaprakash, "Influence of plasma nitriding on plain fatigue and fretting fatigue behavior of AISI 304 austenitic stainless steel," *Surface & Coatings Technology*, vol. 201, pp. 5906–5911, 2007.

[29] B. K. Jones and J. W. Martin, "Residual stress distribution in nitride En41B steel as function of case depth," *Met. Technol*, vol. 4, pp. 520–523, 1977.

[30] T. Bell and N. L. Loh, "The fatigue characteristics of Plasma Nitrided three Pct Cr-Mo steel," *Journal of Heat Treating*, vol. 2, no. 3, pp. 232–237, 1982.

[31] B. K. Jones and J. W. Martin, "Fatigue failure mechanisms in a nitrided En 41B steel," *Metals Technology*, vol. 5, no. 1, pp. 217–221, 1978.

[32] C. Galassi, V. Biasini, and S. Guicciardi, "Correlation between casting parameters and mechanical properties of an Al2O3-ZrO2 composite," *Journal of the European Ceramic Society*, vol. 12, no. 6, pp. 441–448, 1993.

[33] I. Campos, R. Rosas, U. Figueroa, C. VillaVelázquez, A. Meneses, and A. Guevara, "Fracture toughness evaluation using Palmqvist crack models on AISI 1045 borided steels," *Materials Science and Engineering: A*, vol. 488, no. 1-2, pp. 562–568, 2008.

[34] D. Coric, L. Curkovic, and M. M. Renjo, "Statistical analysis of Vickers indentation fracture toughness of Y-TZP ceramics," *Transactions of FAMENA*, vol. 41, 2017.